

Regularized Personalization of Text-to-Image Diffusion Models without Distributional Drift

Gihoon Kim Hyungjin Park Taesup Kim

Graduate School of Data Science, Seoul National University

Abstract

Personalization using text-to-image diffusion models involves adapting a pretrained model to novel subjects with only a few image examples. This task presents a fundamental challenge, as the model must not only learn the new subject effectively but also preserve its ability to generate diverse and coherent outputs across a wide range of prompts. In other words, successful personalization requires integrating new concepts without forgetting previously learned generative capabilities. Forgetting denotes unintended distributional drift, where the model’s output distribution deviates from that of the original pretrained model. In this paper, we provide an analysis of this issue and identify a mismatch between standard training objectives and the goals of personalization. To address this, we propose a new training objective based on a Lipschitz-bounded formulation that explicitly constrains deviation from the pretrained distribution. Our method provides improved control over distributional drift and performs well even in data-scarce scenarios. Experimental results demonstrate that our approach consistently outperforms existing personalization methods, achieving higher CLIP-T, CLIP-I, and DINO scores.

1 Introduction

Recent advances in diffusion-based image generation models have demonstrated remarkable performance [1–7]. In particular, text-to-image models that condition on textual prompts have made significant progress, enabling the synthesis of images from text descriptions across a wide range of contexts [8–11]. While these models excel at synthesizing images that reflect general concepts (e.g., “a dog in the snow”), they struggle to faithfully depict specific, user-provided subjects (e.g., “my dog in the snow”). To address this limitation, personalization methods have been proposed to adapt pretrained diffusion models to user-specific subjects using only a few concept or reference images [12, 13].

The ultimate goal of personalization is to model the distribution of a new and user-specific subject such as “my dog” while preserving the generative diversity encoded in the pretrained model like “in the snow”, thereby enabling diverse image synthesis for that subject. Indeed, studies have shown that pretrained diffusion models are capable of generating even conceptually rare or complex images when provided with appropriate textual or structural conditions [14–17]. From this perspective, personalization can be seen as the task of learning suitable guidance mechanisms, such as prompt conditioning or embedding adaptation, for novel concepts, while remaining within the support of the pretrained distribution. However, in practice, personalized diffusion models often suffer from a clear trade-off: *improving subject fidelity by fitting to the target images causes the model to drift from the pretrained distribution, thereby weakening its ability to align with diverse text prompts.*

Achieving both adaptation and distribution preservation therefore remains a fundamental challenge. Furthermore, training with a few examples makes it difficult to maintain a delicate balance. This sensitivity of the personalization process often results in unintended shift and leads to issues where the model loses its original generative capabilities. Existing methods address these issues by updating

Table 1: Overview of personalization methods. Our approach provides an analytical bound on distribution preservation. It avoids reliance on auxiliary datasets required by encoder-based techniques, and enables explicit trade-off control between subject fidelity and distribution preservation via a single scalar parameter λ .

Method	Dist. Preservation	No Auxiliary Dataset	Trade-off Control
Encoder-based (i.e. IP-Adaptor)	—	×	×
Finetune-based (i.e. Dreambooth)	△	△	×
Ours	○	○	○

a small subset of parameters [13, 18–22]. This approach enables adaptation to new concepts while preserving the integrity of the pretrained model. Yet this approach still faces challenges such as identifying which parameters to update and limited expressiveness resulting from restricted updates, as further demonstrated in experiments in Section 5. Moreover, such methods provide only limited and indirect control over distributional drift.

While prior work has primarily focused on architectural design and parameter selection, the training objective itself remains underexplored. We therefore investigate whether the difficulties observed in personalization stem from an incompatibility between the standard objective and the task requirements. In Section 4.1, we show that the existing objective fails to constrain distributional drift when personalizing to a small subject-specific distribution. While personalization aims to operate within the inductive biases of a pretrained model, there is no guiding principle to preserve such biases. This analysis reveals the need for an alternative objective that better aligns with the goals of personalization. Even though distribution-matching objectives have recently been explored, they still rely on large-scale data and computationally intensive optimization. These prerequisites render them impractical for few-shot personalization, where only 3–5 concept images per subject are available.

Building on these observations, we propose a novel objective function that incorporates Lipschitz-based constraints to regularize the personalization process. Our goal is to enable personalization with guarantees on preserving the pretrained distribution as shown in Table 1. The proposed formulation enables distribution matching without requiring the extensive datasets typically assumed in prior approaches. Moreover, as shown in Section 4.2, it provides an analytical bound on the distribution shift—a property absent in standard personalization objectives. Finally, the results demonstrate that our method achieves strong subject fidelity while preserving the generative versatility of the original model. In addition, the trade-off between adaptation and distribution preservation can be controlled via a single scalar Lipschitz constant, offering both simplicity and interpretability. Our contributions are summarized as follows:

- We identify a fundamental mismatch between the standard personalization objective and the goals of personalization, and show that conventional training leads to distributional drift away from the pretrained model.
- We propose a new training objective based on Lipschitz regularization, which bounds the shift from the pretrained distribution and enables controllable personalization without requiring large-scale data or architectural modifications.
- We validate our method through extensive experiments across diverse subjects, demonstrating superior subject fidelity, validation of the proposed objective, and interpretable control over the adaptation–preservation trade-off.

2 Related Work

Personalized Text-to-Image Generation. Personalization methods can be broadly categorized into two directions. The first is finetuning-based methods [12, 13, 18–25]. Textual Inversion [13, 23] attempts to encode subject-specific information into new text tokens. On the other hand, DreamBooth [12] finetunes the entire U-Net and introduces the prior preservation loss, which we revisit in Section 4.1. Subsequent works aim to improve stability and efficiency by identifying more suitable subsets of U-Net parameters to update. Custom Diffusion [19] and Perfusion [20, 26] constrain updates to the attention layers. Low-rank adaptation (LoRA) [18, 25] is also applied in this context. SVDiff [22] focuses updates on the singular values of weight matrices, while OFT [21] restricts them to angular components. The second direction involves encoder-based methods [27–33]. These approaches enable zero-shot inference across domains by introducing a dedicated encoder to condition

the diffusion model such as ControlNet [33, 34]. However, they often entail substantial computational and parameter overhead. For example, BLIP-Diffusion [27] leverages pretrained vision-language models [35, 36], while IP-Adapter [29] trains an adaptor network on large-scale datasets. Both mainstream directions thus tackle the personalization challenge either by exploring architectural modifications or by integrating auxiliary networks.

Distribution Matching. Recent score distillation methods [37–39] aim to align the output distribution of a learnable generator with that of a pretrained diffusion model. Score Distillation Sampling (SDS) [37] leverages the pretrained diffusion distribution as a guidance prior. Originally proposed for 3D generation [40], SDS has since gained attention for its ability to transfer the pretrained distribution to a variety of downstream tasks. Building on this insight, subsequent works have extended the framework to downstream applications such as image editing [38, 41]. More recent efforts [42–44] move beyond instance-level conditioning and investigate transplanting the rich generative distribution of diffusion models into target generators. To address the inherent mode-seeking behavior of SDS, these methods incorporate pairwise supervision [42] or adversarial objectives [43, 44]. However, these methods rely on large-scale datasets and extensive optimization. These requirements limit their applicability in personalization settings, where only a handful of subject images are available.

3 Background

Text-to-Image Diffusion Models. Denoising diffusion models are trained to maximize an evidence lower bound (ELBO) on the data log-likelihood $\log p(\mathbf{x})$ due to the intractability [45–48]. The generative process is formulated over a sequence of latent variables [45], which can be written as:

$$\log p(\mathbf{x}) = \log \int p(\mathbf{x}_{0:T}) d\mathbf{x}_{1:T} \geq \mathbb{E}_{q(\mathbf{x}_{1:T}|\mathbf{x}_0)} \left[\log \frac{p(\mathbf{x}_{1:T})}{q(\mathbf{x}_{1:T} | \mathbf{x}_0)} \right]. \quad (1)$$

Rather than optimizing Eq. (1) directly, DDPM [2] adopt a surrogate loss for transition-noise prediction. Text-to-Image diffusion frameworks [8, 9, 11] train the denoiser conditioned on a text prompt c , and the resulting conditional surrogate loss maximizes the joint distribution $p_\theta(\mathbf{x}, c)$. This follows from the conditional distribution $\log p_\theta(\mathbf{x} | c) = \log p_\theta(\mathbf{x}, c) - \log p(c) = \log \int p_\theta(\mathbf{x}, \mathbf{z}_{1:T}, c) d\mathbf{z}_{1:T} - \log p(c)$, where $\log p(c)$ is constant with respect to θ . In detail, an encoder \mathcal{E} maps an image \mathbf{x} to a latent $\mathbf{z} = \mathcal{E}(\mathbf{x})$, and noisy latents are generated as $\mathbf{z}_t = \sqrt{\bar{\alpha}_t} \mathbf{z} + \sqrt{1 - \bar{\alpha}_t} \boldsymbol{\epsilon}$, where $\boldsymbol{\epsilon} \sim \mathcal{N}(\mathbf{0}, \mathbf{I})$ and $t \sim \text{Uniform}\{1, \dots, T\}$. Here, $\bar{\alpha}_t$ denotes the cumulative product of the noise schedule. Training then minimizes the conditional noise-prediction loss:

$$\mathcal{L}_{\text{Denoise}} = \mathbb{E}_{\mathbf{z}, \mathbf{c}, \boldsymbol{\epsilon}, t} \|\boldsymbol{\epsilon} - \boldsymbol{\epsilon}_\theta(\mathbf{z}_t, \mathbf{c}, t)\|_2^2. \quad (2)$$

Prior Preservation Loss. DreamBooth [12] propose a prior preservation term. Then, the total training loss becomes $\mathcal{L}_{\text{total}} = \mathcal{L}_{\text{simple}} + \lambda_{\text{prior}} \mathcal{L}_{\text{prior}}$, where each term follows the conditional diffusion objective in Eq. (2). For the personalization loss, c is set to the target prompt (e.g., “A photo of V* dog”), guiding the model to learn the subject-specific features. For the prior loss, c is instead the generic class prompt “A photo of a dog,” and 100–200 class-prompt latents \mathbf{z}'_t are sampled from the pretrained model. The combined objective can be written as:

$$\mathcal{L}_{\text{DB}} = \mathbb{E}_{\mathbf{z}, \mathbf{z}', \mathbf{c}_{\text{target}}, \mathbf{c}_{\text{class}}, \boldsymbol{\epsilon}, t} \left[\|\boldsymbol{\epsilon} - \boldsymbol{\epsilon}_\theta(\mathbf{z}_t, \mathbf{c}_{\text{target}}, t)\|_2^2 + \lambda_{\text{prior}} \|\boldsymbol{\epsilon} - \boldsymbol{\epsilon}_\theta(\mathbf{z}'_t, \mathbf{c}_{\text{class}}, t)\|_2^2 \right]. \quad (3)$$

4 Regularized Personalization without Distributional Drift

In this section, we investigate why the standard objective fails to enable effective learning in personalization. Next, we explore how to provide a distributional bound tailored to preserving the generative capacity of the pre-trained distribution. We first outline the general personalization assumptions and the notation. Let $x \in \mathcal{X}$ denote an image and $c \in \mathcal{C}$ its associated text prompt. The pretraining dataset $D_{\text{base}} = \{(x_i, c_i)\}_{i=1}^N$ is sampled i.i.d. from a distribution $p_{\text{base}}(x, c)$ that closely approximates the true data distribution $p^*(x, c)$. The personalization dataset $D_{\text{per}} = \{(x_j, c_j)\}_{j=1}^M$, with $M \ll N$, has underlying distribution $p_{\text{per}}(x, c)$. Such assumptions are standard and align with practical settings, ranging from large-scale pretraining on LAION-400M [1, 49, 50] to a personalization dataset with only 3–5 images per subject [12].

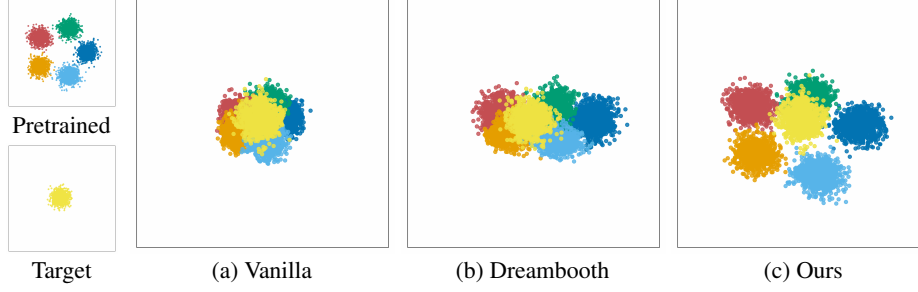


Figure 1: Visualization results from Section 4.3. The diffusion model is first trained on the pretrained dataset and then adapted to the target dataset. (a) and (b), optimized by Eqs. (2) and (3) respectively, fail to preserve the distributions of all classes. In contrast, (c), which incorporates the proposed Lipschitz regularization, better maintains the structure of the pretrained distribution.

4.1 Motivation: Objective–Goal Misalignment

We begin by observing that minimizing the forward KL divergence $D_{KL}(p_{\text{data}} \| p_{\theta})$ is equivalent to maximum-likelihood training under p_{data} . Diffusion models therefore optimize the noise-prediction loss of Eq. (2), thereby driving p_{θ} to match the training distribution p_{data} .

We now show in Theorem 1 that standard personalization using Eq. (2) leads to divergence from the original distribution. This reflects a fundamental misalignment: the goal in personalization is not merely to fit the training distribution, but to preserve the generalization capabilities of the pretrained model while incorporating novel subject information. Moreover, as shown in Corollary 1, this issue persists even under the existing prior preservation strategy defined in Eq. 3.

Theorem 1. *Let $p^*(x, c)$ denote the reference distribution, and let the model parameters θ_{base} have distribution $p_{\theta_{\text{base}}}(x, c)$ satisfying, for any $\epsilon > 0$,*

$$|p^*(x, c) - p_{\theta_{\text{base}}}(x, c)| < \epsilon.$$

The model is adapted by gradient descent on the denoising loss $\mathcal{L}_{\text{Denoise}}$ from Eq. (2), trained on $(x, c) \sim p_{\text{adapt}}$:

$$\theta_{t+1} = \theta_t - \eta \nabla_{\theta} \mathcal{L}_{\text{Denoise}}(\theta_t), \quad \text{where } \theta_0 = \theta_{\text{base}}.$$

Under universal approximation and convergence assumptions [51], after sufficient iterations t ,

$$p_{\theta_t} \longrightarrow p_{\text{adapt}}.$$

Suppose there exists a measurable set $D \subset \mathcal{X} \times \mathcal{C}$ such that

$$p_{\text{adapt}}(D) = \gamma, \quad p^*(D) = \delta, \quad \gamma \gg \delta > 0.$$

Then

$$D_{KL}(p^* \| p_{\theta_{\text{base}}}) < D_{KL}(p^* \| p_{\theta_t}).$$

Proof. See Appendix A. □

Remark 1. The above analysis applies to existing personalization methods in general, suggesting that such methods offer no guarantee of preserving the pretrained distribution and may lead to divergence.

Corollary 1. *Let p_{class} be the sub-distribution of $p(x, c_{\text{class}})$ used for prior preservation as described in Section 3. p'_{per} , a mixture of p_{per} and p_{class} , still satisfies $M \ll N$. Then,*

$$p'_{\text{per}}(D) \geq \gamma', \quad p^*(D) \leq \delta \quad (\gamma' \gg \delta).$$

By Theorem 1,

$$D_{KL}(p^* \| p_{\theta_{\text{base}}}) < D_{KL}(p^* \| p'_{\theta_t}).$$

Remark 2. Even when trained with prior-preservation samples based on the class prompt, as in Eq. 3, the model still offers no guarantee of preserving the pretrained distribution.

Remarks 1 and 2 highlight a fundamental limitation in achieving both subject adaptation and distributional preservation as illustrated in Figures 1a and 1b. It also explains why the unintended distribution shift poses inherent challenges in personalization.

4.2 Lipschitz-based Regularization for Distribution Preservation

Theorem 1 shows that personalization objectives in Eqs. (2) and (3) are insufficient to resolve the trade-off between subject fidelity and distributional generality. We therefore formulate a new training objective by leveraging Lipschitz continuity to provide an explicit bound on distributional preservation. The following Theorem 2 provides the motivation by showing that the generative distribution of the model is bounded under the Lipschitz continuity of the noise prediction network. The detailed proof is deferred to Appendix B.

Theorem 2. *If the diffusion model ε_θ is Lipschitz continuous in θ , then for any two parameter sets θ_1 and θ_2 , there exists a constant $\lambda > 0$ such that*

$$D_{KL}(p_{\theta_1} \| p_{\theta_2}) \leq \lambda \cdot \|\theta_1 - \theta_2\|_k. \quad (4)$$

*Proof sketch.*¹

- Composition of Lipschitz-continuous layers (e.g., convolutions, ReLU) makes $\varepsilon_\theta(x, t)$ Lipschitz in θ [52, 53].
- By Tweedie’s formula [2, 6, 54], the score is $s_\theta(x, t) = -\varepsilon_\theta(x, t)/\sigma_t$, and scalar multiplication by $1/\sigma_t$ preserves Lipschitz continuity.
- The probability-flow ODE [6, 55] gives $\log p_\theta(x) = \log p_T(x_T) - \int_0^T s_\theta(x_t, t) \frac{dx_t}{dt} dt$, and since integration is a linear operator, it also preserves the Lipschitz bound.
- Finally, the triangle inequality implies $D_{KL}(p_{\theta_1} \| p_{\theta_2}) \leq \lambda \|\theta_1 - \theta_2\|_k$.

Remark 3. The Lipschitz regularization on $\|\theta_{\text{per}} - \theta_{\text{base}}\|_k$ provides a bound on the distributional shift from the pretrained distribution during personalization.

Building on Theorem 2, we propose a new objective that augments Eq. (2) with a regularizer on the distance between the pretrained and personalized parameters based on Eq. (4). As a result, our objective both learns the new subject distribution and preserves the pretrained distribution, which the conventional objective is unable to ensure. This aims not only to preserve sub-distributions of specific classes, but also to maintain the general generative capacity of the pretrained distribution as illustrated in Figure 1c. We demonstrate that the proposed Lipschitz-based regularization supports the claim as shown in Figure 2 and Table 3. The full training procedure with the proposed objective is summarized in Algorithm 1. We also show that the proposed objective improves personalization performance by better balancing subject fidelity and distributional preservation in Section 5.3.

The proposed objective also provides practical advantages. First, preserving the distribution through parameter distance does not require large external datasets, unlike distribution matching methods [42–44]. This property makes the approach suitable for the few-shot nature of personalization. Second, the Lipschitz-based regularizer bounds the KL divergence from the pretrained distribution by a single hyperparameter λ , quantifying the degree of distributional preservation during training. This enables explicit control over what previous methods addressed only implicitly through strategies such as freezing parameters or restricting updates. We validate both benefits through a toy experiment and ablation studies.

4.3 Toy Experiment: Method Validation

We conduct a toy experiment to validate the claim in Theorem 2. This experiment investigates how Lipschitz-based regularization influences the preservation of the pretrained distribution when the model adapts to a new target. We employ a shallow diffusion model trained on 2D data sampled from Gaussians with shared variance and different means. As illustrated in Figure 1, five classes are used in the pretraining phase, and a new class is introduced later. The model is first trained with the objective in Eq. (2), and then finetuned with different objectives.

Lipschitz regularization leads to better preservation of the pretrained distribution as shown in Figure 1. When finetuning is performed solely with Eq. (2), the pretrained distribution collapses. Using Eq. (3) partially preserves the selected class (shown in deep blue), but the rest of the pretrained distribution is not maintained. In contrast, when Lipschitz-based regularization is applied as in Algorithm 1, the model better preserves the original distribution while still adapting to the new data. This empirical

¹Following standard practice, we omit the prompt c and write $\varepsilon_\theta(x, t)$ and $\log p_\theta(x)$. All statements extend directly to the conditional case by replacing $\varepsilon_\theta(x, t)$ with $\varepsilon_\theta(x, c, t)$ and $\log p_\theta(x)$ with $\log p_\theta(x, c)$.

Algorithm 1 Lipschitz-Regularized Personalization

Require: Pretrained model $\epsilon_{\theta_{\text{base}}}$, subject dataset $\mathcal{D}_{\text{per}} = \{x_i\}_{i=1}^N$, training prompt c_{per} , weight λ

Ensure: Personalized generator $\epsilon_{\theta_{\text{per}}}$

```
1:  $\epsilon_{\theta_{\text{per}}} \leftarrow \text{copyWeights}(\epsilon_{\theta_{\text{base}}})$ 
2: Freeze teacher model  $\epsilon_{\theta_{\text{base}}}$ 
3: for each training step do
4:   Sample image  $x \sim \mathcal{D}_{\text{per}}$ 
5:    $z \leftarrow \mathcal{E}(x)$ 
6:   Text embedding  $c \leftarrow \text{TextEncoder}(c_{\text{per}})$ 
7:   Sample  $t \sim \mathcal{U}(\{1, \dots, T\})$ ,  $\epsilon \sim \mathcal{N}(0, \mathbf{I})$ 
8:    $\tilde{z}_t \leftarrow \sqrt{\alpha_t}z + \sqrt{1 - \alpha_t}\epsilon$ 
9:    $\mathcal{L}_{\text{Denoise}} \leftarrow \|\epsilon - \epsilon_{\theta_{\text{per}}}(\tilde{z}_t, t, c)\|_2^2$ 
10:   $\mathcal{L}_{\text{Lipschitz}} \leftarrow \sum_i \|\theta_{\text{per}}^i - \theta_{\text{base}}^i\|_k$ 
11:   $\mathcal{L}_{\text{Total}} \leftarrow \mathcal{L}_{\text{Denoise}} + \lambda \mathcal{L}_{\text{Lipschitz}}$ 
12:   $\theta_{\text{per}} \leftarrow \text{update}(\theta_{\text{per}}, \nabla_{\theta_{\text{per}}} \mathcal{L}_{\text{Total}})$ 
13: end for
```

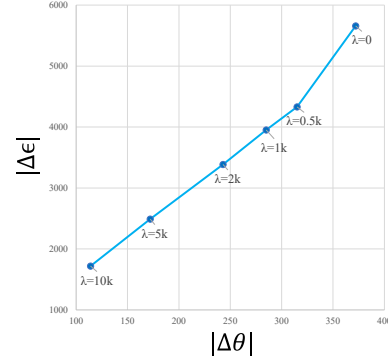


Figure 2: Effect of Lipschitz regularization: Increasing λ reduces both $\Delta\theta$ and $\Delta\epsilon$.

result suggests that, unlike conventional methods that primarily preserve the subject class (e.g., “dog” in “a my dog in the snow”), our approach can retain broader contextual generality (e.g., “the snow”) during personalization. This also demonstrates that the proposed method can maintain the pretrained distribution even without explicit access to the original training data, making it more suitable for personalization scenarios with limited data and complex distributions.

5 Experiments and Results

We assess the effectiveness of our proposed method through both qualitative and quantitative comparisons with baselines. We also conduct an ablation study to determine whether the proposed objective preserves the pretrained distribution and enables controllable trade-offs as claimed in this work.

5.1 Experiments Setup

Implementation details. We evaluate our method and baselines on the widely used personalization benchmark [12], which includes 30 subjects, each with up to 6 example images. We follow the experimental settings reported in each study and use either official implementations or widely adopted open-source code. We train each baseline using its standard hyperparameter configuration, which remains fixed across all subjects. For finetuning-based baselines, we consider DreamBooth [12], Textual Inversion [13], Custom Diffusion [19], SVDiff [22], and OFT [21], as well as an extension based on LoRA [18]. While we attempted to reproduce OFT using the official codebase, it did not produce usable outputs under our setting. As a result, we report its performance based on the results presented in the original paper. We also include encoder-based methods BLIP-Diffusion [27] and IP-Adapter [29] for comprehensive comparisons.

Our method uses Stable Diffusion v1.5 [8] as the base model to ensure consistency with all baselines. Training is performed on 1000 optimization steps. In practice, we implement $\|\cdot\|_k$ as the squared ℓ_2 norm. Due to the small updates caused by the low learning rate, a relatively large scalar is necessary to balance the regularization term. We set the weight λ for the Lipschitz regularization to 500, and perform ablation studies over a comparable scale to evaluate its effect. Our training prompts follow the DreamBooth protocol. Each baseline uses its original prompt setup. When special tokens are required, we apply the same token convention across all methods to ensure a controlled comparison.²

Evaluation Methods. We evaluate each method based on the images generated from evaluation prompts. All images are generated using a fixed random seed over 50 denoising steps with a guidance scale of 7.5. For each subject, we use the 25 evaluation prompts provided in the benchmark, generating 4 images per prompt, resulting in 100 images per subject and a total of 3,000 images across all 30 subjects. We evaluate model performance using three metrics: DINO, CLIP-T, and CLIP-I. We use pretrained DINO ViT-S/16 [56] and CLIP ViT-B/32 [57] models to extract image and text embeddings. CLIP-I and DINO measure subject fidelity by computing the cosine similarity between each generated image and the corresponding input reference images. CLIP-T evaluates

²For details on the setup and implementation of individual experiments, please refer to Appendix C.

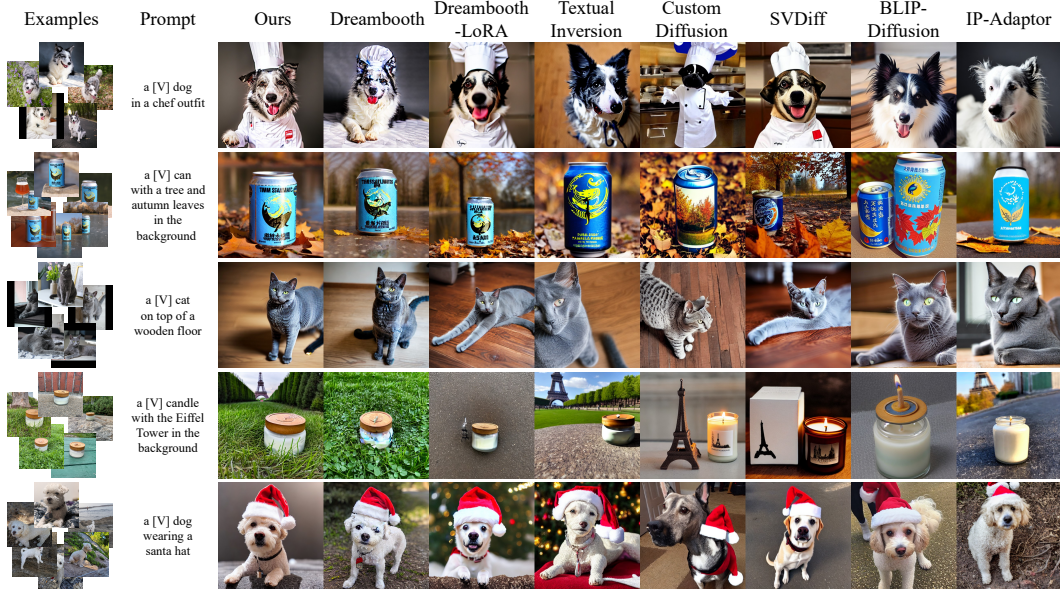


Figure 3: Visual comparison with baseline methods

text-image alignment based on cosine similarity between the prompt and the generated image. The special token is excluded when computing CLIP-T scores.

5.2 Comparisons with Baseline Methods

Qualitative Comparison. The qualitative results are presented in Figure 3 for three live subjects and three objects from the benchmark dataset. Compared to baseline methods, the proposed method demonstrates superior performance in both fidelity and prompt alignment. Among the baselines, DreamBooth and DreamBooth-LoRA show strong performance. However, DreamBooth either fails to incorporate the prompt or exhibits artifacts in rows 1 and 4. DreamBooth-LoRA tends to underrepresent subject identity in rows 1 and 5. We attribute these issues to the trade-off between overfitting in the full-parameter DreamBooth setting and limited expressiveness in the frozen-parameter LoRA setting.

Other methods generally underperform. Textual Inversion struggles to capture fine-grained subject details. Custom Diffusion and SVDiff tend to focus more on prompt alignment than subject fidelity. Encoder-based models such as BLIP-Diffusion and IP-Adapter yield results that contrast with their quantitative performance in Table 2. While the overall structure of the subject is preserved, identity-specific features are often missing. This discrepancy suggests potential limitations in evaluation metrics. The qualitative results show that our method performs well in both image fidelity and text alignment compared to the baselines.

Quantitative Comparison. Table 2 summarizes the quantitative results for the proposed method and baseline models. Our method maintains strong performance across both metrics. No other baseline matches our model in both text and image alignment scores simultaneously. SVDiff, Custom Diffusion, and DreamBooth-LoRA exhibit relatively high CLIP-T scores above 0.3, but their DINO scores remain below 0.6. This suggests that methods that freeze the backbone (either partially or entirely) to prevent distributional drift struggle to adapt to new subject-specific features. On the other hand, encoder-based methods such as IP-Adapter achieve the highest DINO and CLIP-I scores, which indicate strong preservation of the input image but result in low performance on CLIP-T. This suggests that encoder-based models have difficulty adapting flexibly to textual prompts. These observations reveal a clear trade-off between text-image alignment and subject fidelity. Nonetheless, our method achieves a more favorable balance across both dimensions compared to the baselines.

We highlight improvements over DreamBooth, which also optimizes all model parameters. This comparison reveals the critical role of the training objective in personalization. Our method outperforms DreamBooth with a substantial gain of over 0.3 in DINO score, indicating improved image fidelity, and also improves CLIP-T by approximately 0.2. The improvements in both image fidelity

Table 2: Quantitative comparison of baseline methods

Method	Type	DINO \uparrow	CLIP-T \uparrow	CLIP-I \uparrow
Real Images	-	0.7050	-	0.8568
Pretrained	-	-	0.3241	-
Ours	Finetune	0.6394	0.2976	0.7948
DreamBooth	Finetune	0.6028	0.2793	0.7881
DreamBooth-LoRA	Finetune	0.5778	0.3095	0.7731
Textual Inversion	Finetune	0.5342	0.2601	0.7608
Custom Diffusion	Finetune	0.3126	0.3179	0.6479
SVDiff	Finetune	0.3839	0.3194	0.6886
OFT	Finetune	0.6320	0.2370	0.7850
BLIP-Diffusion	Encoder	0.5943	0.2865	0.7935
IP-Adaptor	Encoder	0.6304	0.2635	0.8318

Table 3: ImageNet class generation: IS and FID scores under varying λ

	IS \uparrow	FID \downarrow
Pretrained	44.1 \pm 2.5	-
Dreambooth	39.6 \pm 3.0	41.7
$\lambda = 0.0$	38.7 \pm 3.2	44.9
$\lambda = 0.5$	40.0 \pm 3.2	43.1
$\lambda = 1.0$	40.4 \pm 3.5	42.6
$\lambda = 2.0$	40.3 \pm 3.5	41.8
$\lambda = 5.0$	40.7 \pm 3.5	39.6
$\lambda = 10.0$	41.5 \pm 3.6	37.6

and text alignment are remarkable, considering the commonly observed trade-off between the two in personalization. This suggests that the proposed formulation better preserves the generality of the pretrained distribution, enabling more faithful generation across diverse prompts. These findings provide strong empirical support for the effectiveness of our objective design.

5.3 Ablation Studies

We conduct two ablation studies to examine the practical implications of the proposed formulation in the context of personalized diffusion models. First, we assess whether diffusion models follow our claim during personalization under the assumptions. Second, we show that our method enables control over the balance between image fidelity and text alignment via the regularization strength λ .

Distribution Preservation. To examine whether the Lipschitz continuity holds in diffusion models, we conduct a series of experiments. First, we measure the parameter deviation $\Delta\theta$ and the corresponding output difference $\Delta\epsilon$ between the pretrained and personalized models. To further assess distributional preservation, we generate samples from the personalized model for representative subjects [25]. The prompts correspond to all 1,000 ImageNet classes [58]. All class-wise generations share the same initial noise. We use Inception Score (IS) [59] and Fréchet Inception Distance (FID) [60] as evaluation metrics, where IS captures both the diversity and perceptual quality of generated images, and FID measures the feature-space distance between images generated by the personalized model and images produced by the pretrained model.

Figure 2 illustrates the effect of applying Lipschitz regularization to the personalized diffusion model. As the regularization strength λ increases, both $\Delta\theta$ and $\Delta\epsilon$ decrease proportionally. This behavior indicates that the change in the output of the model is bounded by the change in parameters. Table 3 demonstrates that stronger regularization reduces the degree of distributional drift from the pretrained model. FID decreases while IS increases as λ increases, which aligns with our formulation. This trend shows that the regularization preserves both distributional proximity (FID) and the generative capacity of the original model (IS). We also point out that DreamBooth can potentially distort the feasible generative space while preserving distributional proximity, as reflected in its relatively low IS score and performance in Table 2. These results support our claim that the proposed regularization can bound the distribution of the generated images.

Trade-off Control. We analyze how the proposed Lipschitz regularization affects the quality of personalized outputs. These experiments evaluate the DINO, CLIP-T, and CLIP-I scores across varying values of the regularization weight λ . As shown in Figure 4, the results exhibit a trade-off between image fidelity and text alignment. A larger λ emphasizes CLIP-T, which reflects better alignment with the text prompt and suggests stronger preservation to the pretrained distribution. In contrast, a smaller λ leads to higher DINO and CLIP-I scores, indicating closer adaptation to the target subject in terms of visual fidelity. This suggests that the proposed objective simultaneously addresses both adaptation and preservation while enabling a controllable balance between them.

This trade-off is reflected in Figure 5. As λ increases, the generated images become more aligned with the prompt. However, the images often fail to capture key attributes of the target subject. As λ decreases, the outputs better reflect subject-specific details. At the same time, they either imitate the input images or include visual artifacts. For example, at $\lambda = 10k$, the output shows a novel pose, but subject fidelity is reduced in rows 2 and 3. At $\lambda = 2k$ and $\lambda = 0.5k$, the results show a more balanced trade-off between prompt alignment and subject fidelity. At $\lambda = 0.0$, row 3 demonstrates a successful case. In contrast, rows 1 and 2 contain artifacts or fail to reflect the prompt. These

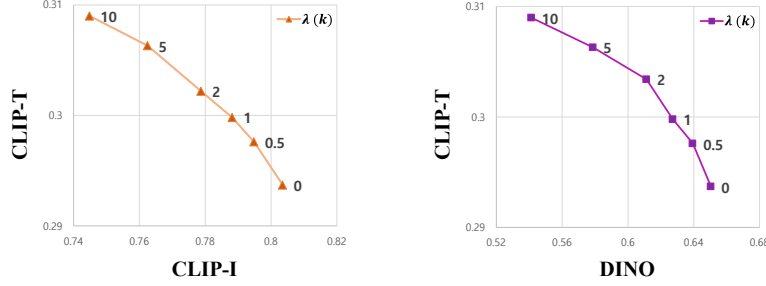


Figure 4: Trade-off curves between image fidelity and text alignment scores across different λ .

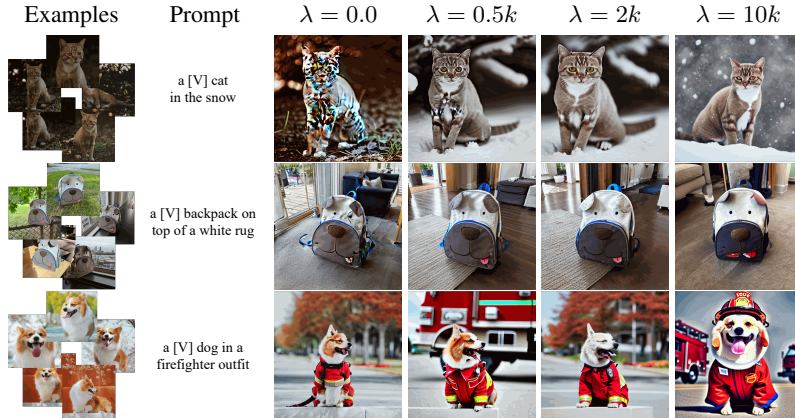


Figure 5: Visual comparison under different regularization strengths. Both $\lambda = 0.5k$ and $\lambda = 2k$ balance identity and prompt alignment.

results suggest that Lipschitz regularization enables explicit control over the trade-off between subject fidelity and prompt alignment. Unlike prior approaches that relied on implicit strategies such as parameter freezing or early stopping, our method offers a principled and flexible way to control image quality in personalized diffusion.

6 Discussion and Future work

We demonstrate that the proposed formulation contributes to the core objectives of personalization by improving both subject fidelity and preserving the pretrained distribution. Empirical findings show that the regularization maintains proximity to the pretrained distribution while improving generation quality. Although our work represents an advance in overcoming earlier limitations, it does not guarantee consistent improvements in performance. In addition, we observe that performance remains variable across subjects. These challenges highlight the need for adaptive personalization training strategies [61, 62]. Future methods should move beyond retaining prior knowledge, toward advancing the integration of novel subject characteristics to achieve more effective and generalizable personalization.

7 Conclusion

We introduce an objective for personalized diffusion models based on Lipschitz regularization. Motivated by the observation that distributional shift can be bounded under a Lipschitz constraint, we formulate a training objective that balances adaptation to novel concepts with preservation of prior knowledge, addressing a core challenge in personalization. Experimental results show that our method improves both image fidelity and textual alignment. Ablation studies further validate the necessity and utility of the proposed regularization. Our method requires no additional data and provides control over the balance between adaptation and preservation. Therefore, our work offers a principled approach to personalization that incorporates new concepts in a manner that better aligns with the goals of personalization without unintended deviation from the pretrained distribution.

References

- [1] Prafulla Dhariwal and Alexander Quinn Nichol. Diffusion models beat gans on image synthesis. *Advances in Neural Information Processing Systems*, 34:8780–8794, 2021.
- [2] Jonathan Ho, Ajay Jain, and Pieter Abbeel. Denoising diffusion probabilistic models. *Advances in neural information processing systems*, 33:6840–6851, 2020.
- [3] Jiaming Song, Chenlin Meng, and Stefano Ermon. Denoising diffusion implicit models. *arXiv preprint arXiv:2010.02502*, 2020.
- [4] Alexander Quinn Nichol and Prafulla Dhariwal. Improved denoising diffusion probabilistic models. In *International conference on machine learning*, pages 8162–8171. PMLR, 2021.
- [5] Jonathan Ho and Tim Salimans. Classifier-free diffusion guidance. *arXiv preprint arXiv:2207.12598*, 2022.
- [6] Yang Song, Jascha Sohl-Dickstein, Diederik P Kingma, Abhishek Kumar, Stefano Ermon, and Ben Poole. Score-based generative modeling through stochastic differential equations. *arXiv preprint arXiv:2011.13456*, 2020.
- [7] Tero Karras, Miika Aittala, Timo Aila, and Samuli Laine. Elucidating the design space of diffusion-based generative models. *Advances in neural information processing systems*, 35:26565–26577, 2022.
- [8] Robin Rombach, Andreas Blattmann, Dominik Lorenz, Patrick Esser, and Björn Ommer. High-resolution image synthesis with latent diffusion models. In *Proceedings of the IEEE/CVF conference on computer vision and pattern recognition*, pages 10684–10695, 2022.
- [9] Chitwan Saharia, William Chan, Saurabh Saxena, Lala Li, Jay Whang, Emily L Denton, Kamyar Ghasemipour, Raphael Gontijo Lopes, Burcu Karagol Ayan, Tim Salimans, et al. Photorealistic text-to-image diffusion models with deep language understanding. *Advances in neural information processing systems*, 35:36479–36494, 2022.
- [10] Aditya Ramesh, Prafulla Dhariwal, Alex Nichol, Casey Chu, and Mark Chen. Hierarchical text-conditional image generation with clip latents. *arXiv preprint arXiv:2204.06125*, 1(2):3, 2022.
- [11] Dustin Podell, Zion English, Kyle Lacey, Andreas Blattmann, Tim Dockhorn, Jonas Müller, Joe Penna, and Robin Rombach. Sdxl: Improving latent diffusion models for high-resolution image synthesis. *arXiv preprint arXiv:2307.01952*, 2023.
- [12] Nataniel Ruiz, Yuanzhen Li, Varun Jampani, Yael Pritch, Michael Rubinstein, and Kfir Aberman. Dream-booth: Fine tuning text-to-image diffusion models for subject-driven generation. In *Proceedings of the IEEE/CVF conference on computer vision and pattern recognition*, pages 22500–22510, 2023.
- [13] Rinon Gal, Yuval Alaluf, Yuval Atzmon, Or Patashnik, Amit H Bermano, Gal Chechik, and Daniel Cohen-Or. An image is worth one word: Personalizing text-to-image generation using textual inversion. *arXiv preprint arXiv:2208.01618*, 2022.
- [14] Shweta Mahajan, Tanzila Rahman, Kwang Moo Yi, and Leonid Sigal. Prompting hard or hardly prompting: Prompt inversion for text-to-image diffusion models. In *Proceedings of the IEEE/CVF Conference on Computer Vision and Pattern Recognition*, pages 6808–6817, 2024.
- [15] Dvir Samuel, Rami Ben-Ari, Simon Raviv, Nir Darshan, and Gal Chechik. Generating images of rare concepts using pre-trained diffusion models. In *Proceedings of the AAAI Conference on Artificial Intelligence*, volume 38, pages 4695–4703, 2024.
- [16] Dvir Samuel, Rami Ben-Ari, Nir Darshan, Haggai Maron, and Gal Chechik. Norm-guided latent space exploration for text-to-image generation. *Advances in Neural Information Processing Systems*, 36:57863–57875, 2023.
- [17] Patrick Schramowski, Manuel Brack, Björn Deiseroth, and Kristian Kersting. Safe latent diffusion: Mitigating inappropriate degeneration in diffusion models. In *Proceedings of the IEEE/CVF Conference on Computer Vision and Pattern Recognition*, pages 22522–22531, 2023.
- [18] Edward J Hu, Yelong Shen, Phillip Wallis, Zeyuan Allen-Zhu, Yuanzhi Li, Shean Wang, Lu Wang, Weizhu Chen, et al. Lora: Low-rank adaptation of large language models. *ICLR*, 1(2):3, 2022.
- [19] Nupur Kumari, Bingliang Zhang, Richard Zhang, Eli Shechtman, and Jun-Yan Zhu. Multi-concept customization of text-to-image diffusion. In *Proceedings of the IEEE/CVF conference on computer vision and pattern recognition*, pages 1931–1941, 2023.

- [20] Yoad Tewel, Rinon Gal, Gal Chechik, and Yuval Atzmon. Key-locked rank one editing for text-to-image personalization. In *ACM SIGGRAPH 2023 conference proceedings*, pages 1–11, 2023.
- [21] Zeju Qiu, Weiyang Liu, Haiwen Feng, Yuxuan Xue, Yao Feng, Zhen Liu, Dan Zhang, Adrian Weller, and Bernhard Schölkopf. Controlling text-to-image diffusion by orthogonal finetuning. *Advances in Neural Information Processing Systems*, 36:79320–79362, 2023.
- [22] Ligong Han, Yinxiao Li, Han Zhang, Peyman Milanfar, Dimitris Metaxas, and Feng Yang. Svdiff: Compact parameter space for diffusion fine-tuning. In *Proceedings of the IEEE/CVF International Conference on Computer Vision*, pages 7323–7334, 2023.
- [23] Andrey Voynov, Qinghao Chu, Daniel Cohen-Or, and Kfir Aberman. p+: Extended textual conditioning in text-to-image generation. *arXiv preprint arXiv:2303.09522*, 2023.
- [24] Shwetha Ram, Tal Neiman, Qianli Feng, Andrew Stuart, Son Tran, and Trishul Chilimbi. Dreamblend: Advancing personalized fine-tuning of text-to-image diffusion models. 2025.
- [25] Shangyu Chen, Zizheng Pan, Jianfei Cai, and Dinh Phung. Para: Personalizing text-to-image diffusion via parameter rank reduction. *arXiv preprint arXiv:2406.05641*, 2024.
- [26] Kevin Meng, David Bau, Alex Andonian, and Yonatan Belinkov. Locating and editing factual associations in gpt. *Advances in neural information processing systems*, 35:17359–17372, 2022.
- [27] Dongxu Li, Junnan Li, and Steven Hoi. Blip-diffusion: Pre-trained subject representation for controllable text-to-image generation and editing. *Advances in Neural Information Processing Systems*, 36:30146–30166, 2023.
- [28] Yuxiang Wei, Yabo Zhang, Zhilong Ji, Jinfeng Bai, Lei Zhang, and Wangmeng Zuo. Elite: Encoding visual concepts into textual embeddings for customized text-to-image generation. In *Proceedings of the IEEE/CVF International Conference on Computer Vision*, pages 15943–15953, 2023.
- [29] Wenhui Chen, Hexiang Hu, Yandong Li, Nataniel Ruiz, Xuhui Jia, Ming-Wei Chang, and William W Cohen. Subject-driven text-to-image generation via apprenticeship learning. *Advances in Neural Information Processing Systems*, 36:30286–30305, 2023.
- [30] Xichen Pan, Li Dong, Shaohan Huang, Zhiliang Peng, Wenhui Chen, and Furu Wei. Kosmos-g: Generating images in context with multimodal large language models. In *The Twelfth International Conference on Learning Representations*.
- [31] Jian Ma, Junhao Liang, Chen Chen, and Haonan Lu. Subject-diffusion: Open domain personalized text-to-image generation without test-time fine-tuning. In *ACM SIGGRAPH 2024 Conference Papers*, pages 1–12, 2024.
- [32] Emanuele Aiello, Umberto Michieli, Diego Valsesia, Mete Ozay, and Enrico Magli. Dream-cache: Finetuning-free lightweight personalized image generation via feature caching. *arXiv preprint arXiv:2411.17786*, 2024.
- [33] Lvmin Zhang, Anyi Rao, and Maneesh Agrawala. Adding conditional control to text-to-image diffusion models. In *Proceedings of the IEEE/CVF international conference on computer vision*, pages 3836–3847, 2023.
- [34] Chong Mou, Xintao Wang, Liangbin Xie, Yanze Wu, Jian Zhang, Zhongang Qi, and Ying Shan. T2i-adapter: Learning adapters to dig out more controllable ability for text-to-image diffusion models. In *Proceedings of the AAAI conference on artificial intelligence*, volume 38, pages 4296–4304, 2024.
- [35] Junnan Li, Dongxu Li, Caiming Xiong, and Steven Hoi. Blip: Bootstrapping language-image pre-training for unified vision-language understanding and generation. In *International conference on machine learning*, pages 12888–12900. PMLR, 2022.
- [36] Junnan Li, Dongxu Li, Silvio Savarese, and Steven Hoi. Blip-2: Bootstrapping language-image pre-training with frozen image encoders and large language models. In *International conference on machine learning*, pages 19730–19742. PMLR, 2023.
- [37] Ben Poole, Ajay Jain, Jonathan T Barron, and Ben Mildenhall. Dreamfusion: Text-to-3d using 2d diffusion. *arXiv preprint arXiv:2209.14988*, 2022.
- [38] Amir Hertz, Kfir Aberman, and Daniel Cohen-Or. Delta denoising score. In *Proceedings of the IEEE/CVF International Conference on Computer Vision*, pages 2328–2337, 2023.

- [39] Zhengyi Wang, Cheng Lu, Yikai Wang, Fan Bao, Chongxuan Li, Hang Su, and Jun Zhu. Prolificdreamer: High-fidelity and diverse text-to-3d generation with variational score distillation. *Advances in Neural Information Processing Systems*, 36:8406–8441, 2023.
- [40] Ben Mildenhall, Pratul P Srinivasan, Matthew Tancik, Jonathan T Barron, Ravi Ramamoorthi, and Ren Ng. Nerf: Representing scenes as neural radiance fields for view synthesis. *Communications of the ACM*, 65(1):99–106, 2021.
- [41] Zhengyang Yu, Zhaoyuan Yang, and Jing Zhang. Dreamsteerer: Enhancing source image conditioned editability using personalized diffusion models. *Advances in Neural Information Processing Systems*, 37:120699–120734, 2024.
- [42] Tianwei Yin, Michaël Gharbi, Richard Zhang, Eli Shechtman, Fredo Durand, William T Freeman, and Taesung Park. One-step diffusion with distribution matching distillation. In *Proceedings of the IEEE/CVF conference on computer vision and pattern recognition*, pages 6613–6623, 2024.
- [43] Tianwei Yin, Michaël Gharbi, Taesung Park, Richard Zhang, Eli Shechtman, Fredo Durand, and Bill Freeman. Improved distribution matching distillation for fast image synthesis. *Advances in neural information processing systems*, 37:47455–47487, 2024.
- [44] Axel Sauer, Dominik Lorenz, Andreas Blattmann, and Robin Rombach. Adversarial diffusion distillation. In *European Conference on Computer Vision*, pages 87–103. Springer, 2024.
- [45] Jascha Sohl-Dickstein, Eric Weiss, Niru Maheswaranathan, and Surya Ganguli. Deep unsupervised learning using nonequilibrium thermodynamics. In *International conference on machine learning*, pages 2256–2265. pmlr, 2015.
- [46] Stanley Chan et al. Tutorial on diffusion models for imaging and vision. *Foundations and Trends® in Computer Graphics and Vision*, 16(4):322–471, 2024.
- [47] Calvin Luo. Understanding diffusion models: A unified perspective. *arXiv preprint arXiv:2208.11970*, 2022.
- [48] Preetum Nakkiran, Arwen Bradley, Hattie Zhou, and Madhu Advani. Step-by-step diffusion: An elementary tutorial. *arXiv preprint arXiv:2406.08929*, 2024.
- [49] Christoph Schuhmann, Richard Vencu, Romain Beaumont, Robert Kaczmarczyk, Clayton Mullis, Aarush Katta, Theo Coombes, Jenia Jitsev, and Aran Komatsuzaki. Laion-400m: Open dataset of clip-filtered 400 million image-text pairs. *arXiv preprint arXiv:2111.02114*, 2021.
- [50] Christoph Schuhmann, Romain Beaumont, Richard Vencu, Cade Gordon, Ross Wightman, Mehdi Cherti, Theo Coombes, Aarush Katta, Clayton Mullis, Mitchell Wortsman, et al. Laion-5b: An open large-scale dataset for training next generation image-text models. *Advances in neural information processing systems*, 35:25278–25294, 2022.
- [51] Yann LeCun, Yoshua Bengio, and Geoffrey Hinton. Deep learning. *nature*, 521(7553):436–444, 2015.
- [52] Behnam Neyshabur, Ryota Tomioka, and Nathan Srebro. Norm-based capacity control in neural networks. In *Conference on learning theory*, pages 1376–1401. PMLR, 2015.
- [53] Kavosh Asadi, Dipendra Misra, and Michael Littman. Lipschitz continuity in model-based reinforcement learning. In *International Conference on Machine Learning*, pages 264–273. PMLR, 2018.
- [54] Bradley Efron. Tweedie’s formula and selection bias. *Journal of the American Statistical Association*, 106(496):1602–1614, 2011.
- [55] Yang Song and Stefano Ermon. Generative modeling by estimating gradients of the data distribution. *Advances in neural information processing systems*, 32, 2019.
- [56] Mathilde Caron, Hugo Touvron, Ishan Misra, Hervé Jégou, Julien Mairal, Piotr Bojanowski, and Armand Joulin. Emerging properties in self-supervised vision transformers. In *Proceedings of the IEEE/CVF international conference on computer vision*, pages 9650–9660, 2021.
- [57] Alec Radford, Jong Wook Kim, Chris Hallacy, Aditya Ramesh, Gabriel Goh, Sandhini Agarwal, Girish Sastry, Amanda Askell, Pamela Mishkin, Jack Clark, et al. Learning transferable visual models from natural language supervision. In *International conference on machine learning*, pages 8748–8763. PmLR, 2021.

- [58] Jia Deng, Wei Dong, Richard Socher, Li-Jia Li, Kai Li, and Li Fei-Fei. Imagenet: A large-scale hierarchical image database. In *2009 IEEE conference on computer vision and pattern recognition*, pages 248–255. Ieee, 2009.
- [59] Tim Salimans, Ian Goodfellow, Wojciech Zaremba, Vicki Cheung, Alec Radford, and Xi Chen. Improved techniques for training gans. *Advances in neural information processing systems*, 29, 2016.
- [60] Martin Heusel, Hubert Ramsauer, Thomas Unterthiner, Bernhard Nessler, and Sepp Hochreiter. Gans trained by a two time-scale update rule converge to a local nash equilibrium. *Advances in neural information processing systems*, 30, 2017.
- [61] James Kirkpatrick, Razvan Pascanu, Neil Rabinowitz, Joel Veness, Guillaume Desjardins, Andrei A Rusu, Kieran Milan, John Quan, Tiago Ramalho, Agnieszka Grabska-Barwinska, et al. Overcoming catastrophic forgetting in neural networks. *Proceedings of the national academy of sciences*, 114(13):3521–3526, 2017.
- [62] Kavosh Asadi, Rasool Fakoor, Omer Gottesman, Taesup Kim, Michael Littman, and Alexander J Smola. Faster deep reinforcement learning with slower online network. *Advances in Neural Information Processing Systems*, 35:19944–19955, 2022.
- [63] Frank Nielsen, Jean-Daniel Boissonnat, and Richard Nock. Bregman voronoi diagrams: Properties, algorithms and applications. *arXiv preprint arXiv:0709.2196*, 2007.
- [64] TM Cover and JA Thomas. Elements of information theory 2nd ed., 2006.

Appendix

A Proof of Theorem 1

Theorem 1. Let $p^*(x, c)$ denote the reference distribution, and let the model parameters θ_{base} have distribution $p_{\theta_{\text{base}}}(x, c)$ satisfying, for any $\epsilon > 0$,

$$|p^*(x, c) - p_{\theta_{\text{base}}}(x, c)| < \epsilon.$$

The model is adapted by gradient descent on the denoising loss $\mathcal{L}_{\text{Denoise}}$ from Eq. (2), trained on $(x, c) \sim p_{\text{adapt}}$:

$$\theta_{t+1} = \theta_t - \eta \nabla_{\theta} \mathcal{L}_{\text{Denoise}}(\theta_t), \quad \text{where } \theta_0 = \theta_{\text{base}}.$$

Under universal approximation and convergence assumptions [51], after sufficient iterations t ,

$$p_{\theta_t} \longrightarrow p_{\text{adapt}}.$$

Suppose there exists a measurable set $D \subset \mathcal{X} \times \mathcal{C}$ such that

$$p_{\text{adapt}}(D) = \gamma, \quad p^*(D) = \delta, \quad \gamma \gg \delta > 0.$$

Then

$$D_{KL}(p^* \| p_{\theta_{\text{base}}}) < D_{KL}(p^* \| p_{\theta_t}).$$

Proof. By the three-point property of Bregman divergences [63], we get

$$D_{KL}(p^* \| p_{\theta_t}) = D_{KL}(p^* \| p_{\theta_{\text{base}}}) + D_{KL}(p_{\theta_{\text{base}}} \| p_{\theta_t}) + \langle p^* - p_{\theta_{\text{base}}}, \log(p_{\theta_t}) - \log(p_{\theta_{\text{base}}}) \rangle.$$

Applying the Cauchy–Schwarz inequality to the rightmost term,

$$|\langle p^* - p_{\theta_{\text{base}}}, \log(p_{\theta_t}) - \log(p_{\theta_{\text{base}}}) \rangle| \leq \|p^* - p_{\theta_{\text{base}}}\| \|\log(p_{\theta_t}) - \log(p_{\theta_{\text{base}}})\|.$$

It follows from the convergence assumption that

$$\|\log(p_{\theta_t}) - \log(p_{\theta_{\text{base}}})\| < M \quad (M < \infty).$$

Then,

$$\|p^* - p_{\theta_{\text{base}}}\| \|\log(p_{\theta_t}) - \log(p_{\theta_{\text{base}}})\| < \epsilon M,$$

the inner-product term is negligible.

Hence,

$$D_{KL}(p^* \| p_{\theta_t}) \approx D_{KL}(p^* \| p_{\theta_{\text{base}}}) + D_{KL}(p_{\theta_{\text{base}}} \| p_{\theta_t}).$$

Applying Pinsker’s inequality [64] on the biased region D we obtain

$$D_{KL}(p_{\theta_{\text{base}}} \| p_{\theta_t}) \geq 2(\gamma - \delta)^2.$$

Then,

$$D_{KL}(p^* \| p_{\theta_{\text{base}}}) + D_{KL}(p_{\theta_{\text{base}}} \| p_{\theta_t}) \geq D_{KL}(p^* \| p_{\theta_{\text{base}}}) + 2(\gamma - \delta)^2.$$

Putting everything together, we obtain

$$\begin{aligned} D_{KL}(p^* \| p_{\theta_t}) &= D_{KL}(p^* \| p_{\theta_{\text{base}}}) + D_{KL}(p_{\theta_{\text{base}}} \| p_{\theta_t}) + \langle p^* - p_{\theta_{\text{base}}}, p'_{\theta_t} - p'_{\theta_{\text{base}}} \rangle. \\ &\approx D_{KL}(p^* \| p_{\theta_{\text{base}}}) + D_{KL}(p_{\theta_{\text{base}}} \| p_{\theta_t}) \\ &\geq D_{KL}(p^* \| p_{\theta_{\text{base}}}) + 2(\gamma - \delta)^2 \\ &> D_{KL}(p^* \| p_{\theta_{\text{base}}}). \end{aligned}$$

Then,

$$D_{KL}(p^* \| p_{\theta_{\text{base}}}) < D_{KL}(p^* \| p_{\theta_t}),$$

as claimed. \square

B Proof of Theorem 2

Theorem 2. If the diffusion model ε_θ is Lipschitz continuous in θ , then for any two parameter sets θ_1 and θ_2 , there exists a constant $\lambda > 0$ such that

$$D_{KL}(p_{\theta_1} \| p_{\theta_2}) \leq \lambda \cdot \|\theta_1 - \theta_2\|_k. \quad (5)$$

Proof. Since deep neural networks are composed of Lipschitz-continuous layers (e.g., convolutions, ReLU) [52, 53, 62], it follows that $\varepsilon_\theta(x, t)$ is Lipschitz in θ . Hence for all x, t and any θ_1, θ_2 ,

$$\|\varepsilon_{\theta_1}(x, t) - \varepsilon_{\theta_2}(x, t)\| \leq L \|\theta_1 - \theta_2\|_k.$$

By Tweedie's formula [2, 6, 54],

$$s_\theta(x, t) = -\frac{\varepsilon_\theta(x, t)}{\sigma_t}.$$

Scalar multiplication preserves Lipschitz continuity, so

$$\|s_{\theta_1}(x, t) - s_{\theta_2}(x, t)\| \leq L' \|\theta_1 - \theta_2\|_k.$$

It follows that s_θ is Lipschitz in θ with constant $L' = L \sup_t \sigma_t^{-1}$.

By the probability-flow ODE formulation [6, 55],

$$\log p_\theta(x) = \log p_T(x_T) - \int_0^T s_\theta(x_t, t) \frac{dx_t}{dt} dt.$$

Since $\log p_T(x_T)$ is constant with respect to θ and integration preserves Lipschitz continuity,

$$|\log p_{\theta_1}(x) - \log p_{\theta_2}(x)| \leq L'' \|\theta_1 - \theta_2\|_k \quad \text{for } \forall x \in X$$

holds with $L'' = \int_0^T L' dt = L \int_0^T \sigma_t^{-1} dt$.

Applying the triangle inequality to the definition of KL divergence then gives

$$\begin{aligned} D_{KL}(p_{\theta_1} \| p_{\theta_2}) &= \int p_{\theta_1}(x) (\log p_{\theta_1}(x) - \log p_{\theta_2}(x)) dx \\ &\leq \int p_{\theta_1}(x) |\log p_{\theta_1}(x) - \log p_{\theta_2}(x)| dx \\ &\leq L'' \|\theta_1 - \theta_2\|_k. \end{aligned}$$

This completes the proof with $\lambda = L''$. □

C Additional Implementation Details

Ours. All experiments are conducted on a single NVIDIA RTX 3090 GPU with a batch size of 1 and a learning rate of 2×10^{-6} , which requires approximately 30 minutes of training per subject. We use the AdamW optimizer and the special token `sk`, which was proposed in DreamBooth and has since become widely adopted. For the proposed Lipschitz-bound regularization, we compare both the L_1 and L_2 norm variants and observe no meaningful difference in performance; accordingly, we adopt the more widely used L_2 norm. We also experiment with integrating DreamBooth’s prior-preservation loss but do not obtain improvements, suggesting a conflict between the objectives. Finally, to compute the Lipschitz regularization in a memory-efficient manner, we iterate through each model parameter in a loop and accumulate its norm.

Baselines. We provide additional implementation details for the baselines used in our experiments in Section 5. The proposed method and DreamBooth are implemented and trained based on the Diffusers library³. For Textual Inversion [13]⁴, Custom Diffusion [19]⁵, SVDiff [22]⁶, and LoRA [18]⁷, we use available implementations and follow their default training settings. OFT [21]⁸ is trained using the official codebase, but we observed poor performance and were unable to fully reproduce the reported results; hence, we cite the numbers from the original paper. BLIP-Diffusion [27]⁹ and IP-Adapter [29]¹⁰ are evaluated using the released model weights on our benchmark through direct inference.

Ablation Studies. We provide additional implementation details for the ablation studies on our proposed personalization process in Section 5.3. Following the same training configuration as in Section 5, we fix the learning rate and number of training iterations, varying only the regularization strength λ for the experiments measuring changes from the pretrained model (i.e., $\Delta\theta$ and $\Delta\epsilon$). For $\Delta\epsilon$, we measure the L2 distance between outputs generated using the unconditional class token from the pretrained and personalized models. The reported value is the accumulated L2 distance over all sampled outputs. For the ImageNet class generation experiments, we generate images using class names from the ImageNet label set, where underscores are replaced with spaces (e.g., `tiger_shark` \rightarrow `tiger shark`). No additional prompt engineering is applied beyond the raw class name.

Toy Experiment. We validate our method using the toy 2D conditional diffusion model as described in Section 4.3. The setup generates 1000 samples per class from 2D Gaussian distributions with a standard deviation of 0.5. Class labels range from 0 to 4, positioned at the vertices of a regular pentagon. A new sixth class (class 5) supports finetuning. The noise schedule follows a cosine-based formulation with $T = 100$ timesteps. The model uses a one-hidden-layer MLP with ReLU activation and class/time embeddings. Initial training runs for 1000 iterations to capture the base distribution effectively. Training for the new class is conducted for 5000 iterations to ensure convergence within the experimental setup. We adopt a DreamBooth-like setup by jointly training the new class with class 0 (deep blue) data. Considering the problem’s complexity, we assign a large weight 100 to class 0 in order to clearly observe the effect of different objectives. When using smaller weights, the other classes tend to collapse toward the new data distribution. However, with weight 100, the objective’s influence on class 0 becomes apparent. For our proposed method, we apply Lipschitz regularization with respect to the pretrained weights, using a regularization strength of $\lambda = 1$. Despite the relatively small weight on regularization, the effect of the objective is clearly reflected in this setup.

³<https://github.com/huggingface/diffusers>

⁴https://github.com/huggingface/diffusers/tree/main/examples/textual_inversion

⁵https://github.com/huggingface/diffusers/tree/main/examples/custom_diffusion

⁶<https://github.com/mkshing/svdif-pytorch>

⁷https://github.com/huggingface/peft/tree/main/examples/lora_dreambooth

⁸<https://github.com/zqiu24/oft>

⁹<https://github.com/salesforce/LAVIS/tree/main/projects/blip-diffusion>

¹⁰<https://github.com/tencent-ailab/IP-Adapter>

D Additional Visual Comparison and Failure Cases

We present additional qualitative results and failure cases. As shown in Figures 6 and 7, our method captures both subject-specific features and prompt semantics. In contrast, DreamBooth often produces artifacts or fails to reflect the prompt, while DreamBooth-LoRA tends to preserve the prompt but underrepresents subject identity. Other baseline methods generally struggle to produce coherent results. We also highlight representative failure cases. Figure 8 shows a case where the model learns the subject’s color but fails to reconstruct its structural identity. In Figure 9, the model fails to properly apply the prompt to the subject. These cases indicate that our method also faces challenges in generating certain subject–prompt combinations. As discussed in Section 6, this underscores the importance of incorporating the distributional structure of both the pretrained model and the target subject.

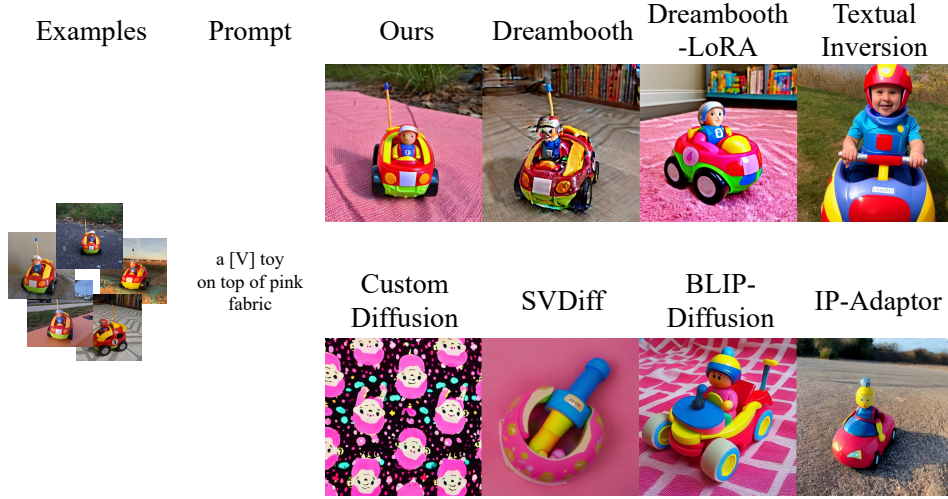


Figure 6: Additional visual Comparison with other baselines.



Figure 7: Additional visual Comparison with other baselines 2.

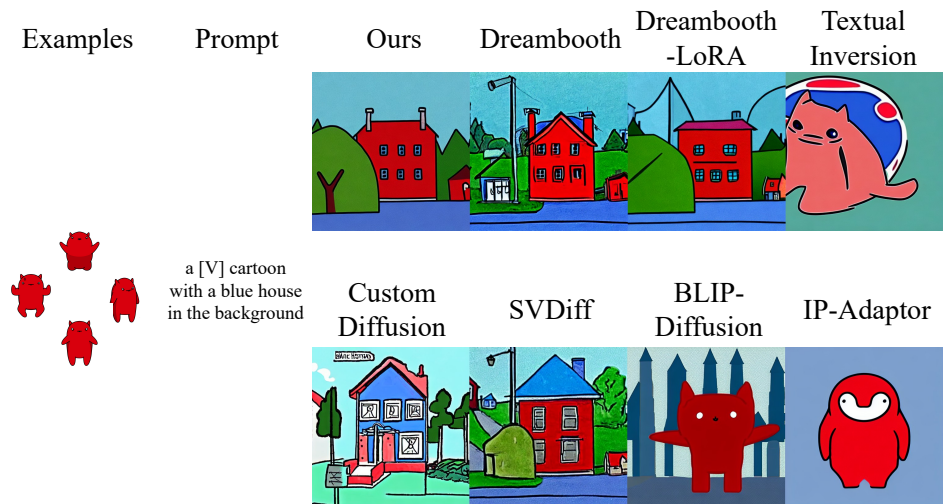


Figure 8: Visual comparison of failure cases across baselines.



Figure 9: Visual comparison of failure cases across baselines 2.

E Additional Comparison with DreamBooth

We conduct an additional experiment using DreamBooth. It is the most comparable method since it finetunes all parameters as our method does. To compare the effect of the objective, we unify all hyperparameters except the loss. We set the learning rate of DreamBooth to 2×10^{-6} , the same as ours, instead of its default 5×10^{-6} . The results are shown in Table 4. Lowering the learning rate in DreamBooth leads to an imbalanced outcome. It improves the CLIP-T score, but lowers both DINO and CLIP-I scores. This suggests reduced image fidelity. As shown in Figure 10, the visual results fail to preserve subject identity in rows 1 and 3, although this is not always the case, as seen in row 2. These findings highlight the difference in objectives. Our method achieves better trade-offs and is more suitable for personalization.

Figures 11 and 12 present ImageNet-class generations from the ablation study. As λ increases, the generated images tend to align more closely with the pretrained distribution. However, since personalization shifts the output distribution, care must be taken when interpreting distributional proximity. Interestingly, in Figure 11, DreamBooth fails to preserve the semantic meaning of the class `tiger shark`, producing generic tiger-like images instead. This serves as a concrete example of the risk of unintended distributional shift.

Table 4: Additional quantitative comparison of personalization methods. All scores are identical to those reported above, except for the last row.

Method	DINO \uparrow	CLIP-T \uparrow	CLIP-I \uparrow
Real Images	0.7050	-	0.8568
Pretrained	-	0.3241	-
Ours	0.6394	0.2976	0.7948
DreamBooth	0.6028	0.2793	0.7881
DreamBooth (LR 2×10^{-6})	0.5707	0.3104	0.7695

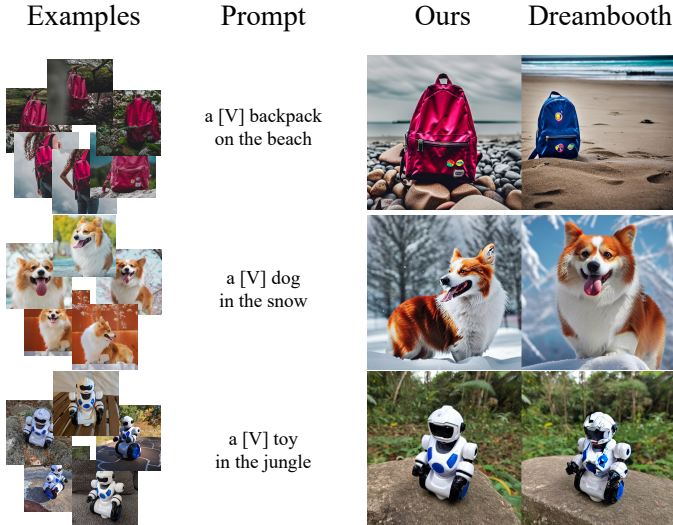


Figure 10: Additional visual Comparison with other baselines.

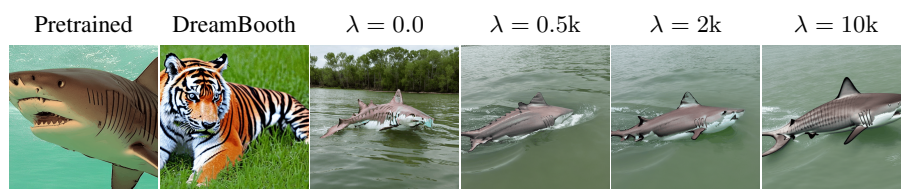


Figure 11: ImageNet class generation: In the case of the "tiger shark" class, DreamBooth generates semantically incorrect images, such as combining a tiger and a shark. This indicates a failure to preserve the semantic priors encoded in the pretrained model, resulting from distributional drift during personalization.

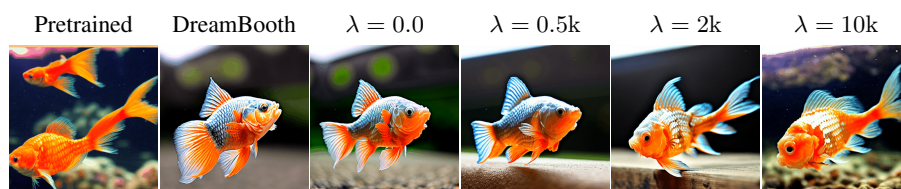


Figure 12: ImageNet class generation: In the case of the "gold fish" class, we observe that increasing the regularization constant produces an image more closely resembling the pretrained model's output; however, it remains noticeably different even at high regularization values.

F Ablation on the Toy Experiment

We conduct an ablation on the Toy Experiment introduced in Section 4.3 to visualize the trend of the proposed method. As shown in Figure 13, the relationship between the newly learned distribution and the original one varies with the regularization strength λ . Without Lipschitz regularization, all classes tend to collapse toward the newly introduced distribution. Notably, even with $\lambda = 1$, the regularization effect becomes evident. In addition, increasing λ progressively enforces preservation of the original distribution, and the newly learned class is mapped closer to one of the existing modes. These results demonstrate that the proposed objective effectively encourages distribution preservation and supports the balancing behavior observed in Section 5.3.

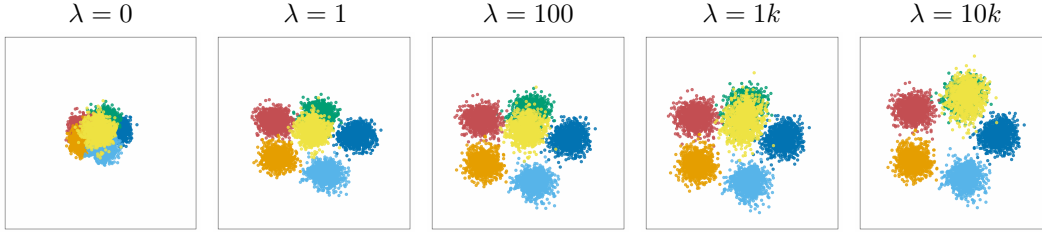


Figure 13: Visualization results under different regularization strengths λ .

G Visual Comparison of Different Class Generations

We present generation results for the *cat* class using personalized models trained on non-cat subjects as shown in Figure 14. Starting from the rightmost pretrained samples, we observe that similarity to the pretrained distribution decreases as λ becomes smaller. In contrast, larger λ values preserve more of the original semantics. This demonstrates that λ controls the degree of distribution preservation.

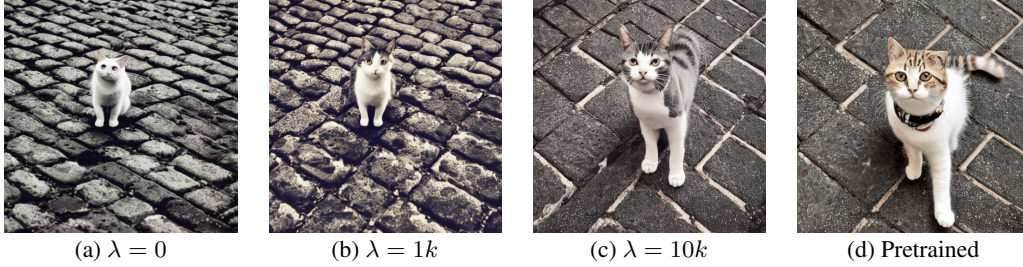


Figure 14: Visualization of ablated results under different λ .

H Broader Societal Impacts

Although our work takes an analytical approach, the broader field of personalized image generation requires careful consideration due to possible misuse. These models could be used to create misleading or harmful images, which may negatively affect individuals or society. This highlights the need to consider ethical implications alongside technical progress in this area of research.

I Additional Discussion

We provide a further discussion on the relationship between evaluation metrics and the claims made in diffusion-based personalization models. Our method introduces a flexible mechanism to balance image fidelity and text alignment. As a result, we observe model variants that score higher in either image fidelity or text alignment. While the main paper is structured around results that show improvements across all metrics, we also observed that some variants with slightly lower image scores but higher CLIP-T scores appeared qualitatively more aligned with the prompts. Although this observation is subjective, it raises an interesting dilemma. Emphasizing quantitative improvements can make the overall claim more convincing, but it may also obscure qualitative alignment that matters for personalization. This underscores a broader challenge in diffusion research: the ambiguity and limitations of current metrics. We believe this calls for a deeper examination of how evaluation metrics are used and interpreted in generative modeling.